HOLLOW PELLETS FOR MAGNETIC FUSION

Zhehui Wang, M. A. Hoffbauer
Los Alamos National Laboratory
Los Alamos, NM 87545, USA
Email: zwang@lanl.gov

E. M. Hollmann
University of California -- San Diego
La Jolla, CA 92093, USA

Y. M. Wang, J. S. Hu
Institute of Plasma Physics, Chinese Academy of Sciences
Hefei, AH 230031, China

R. Maingi, J. E. Menard
Princeton Plasma Physics Laboratory
Princeton, NJ 08544, USA

X. Q. Xu
Lawrence Livermore National Laboratory
Livermore, CA 94550, USA

Abstract

Precise delivery of mass to magnetic fusion plasmas is a problem of growing interest. The answers to how much mass is necessary and sufficient can vary depending on parameters such as the type of atoms involved, the type of application, plasma condition, the mass injector, and injection timing. Motivated by edge localized mode (ELM) control in H-mode plasmas, we describe a new form of mass delivery based on hollow pellets. We recognize past and ongoing work in using shell pellets for disruption mitigation and diagnostics. Here, a hollow pellet refers to a layered spherical structure with a hollow core. Based on empirical models of pellet ablation, coupled with BOUT++ simulations of ELM triggering, hollow pellets are found to be attractive in comparison with solid spheres. By using hollow pellets, it is possible to tailor mass delivery to certain regions of edge plasmas while minimizing core contamination and reducing the amount of mass needed. There are known discrepancies between theoretical predictions and experiments in using mass injection for ELM control, which warrant experiments using hollow pellets. For example, the amount of mass or the number of atoms to reliably trigger ELM was predicted to be more than 10^{20} particles in existing machines, while experimental observations showed smaller quantities. We also include experimental progress in mass delivery experiment, in-situ diagnostics and hollow pellet fabrication, and highlight some new possibilities for experimental demonstration of ELM control based on hollow pellets.

1. INTRODUCTION

Edge localized modes (ELMs) are the signature of high-confinement or H-mode plasmas. An H-mode mode plasma is associated with a steep edge plasma pressure gradient and the spontaneous bootstrap current, or the `edge pedestal' which provides a transport barrier to improve the particle and energy confinement as well as mechanisms for natural ELMs and other MHD instabilities. The amount of energy released by ELMs is proportional to the stored plasma energy and can exceed 10% in the extreme cases. Natural ELMs in ITER and alike can potentially accelerate the plasma facing wall deterioration and ELM control is therefore necessary for ITER and future fusion reactors [1-5]. Several approaches such as mass injection and 3D edge magnetic field have experimentally shown to be feasible in inducing ELMs at a frequency higher than the natural ELM frequency of a few Hz and reduce the peak energy flux onto the divertor and other surfaces. Both physics as well as technological questions remain regarding the ELM controls. We compare the effects of different mass injection techniques here for ELM control and conclude that layered spherical structures with a hollow core, `hollow pellets', are attractive in ELM control when compared with existing solid spheres and gas puffing. Prototype layered structures of boron and polymers have been fabricated and characterized.

Open questions related to ELM control by mass injection include the amount of mass needed, the timing of the mass injection with respect to the natural ELM cycle and location of the mass injection with respect to the magnetic flux surfaces and the edge pedestal, and the correlations between the injected mass properties with the

induced ELM amplitude, and the size of ELM footprint. Experimental results from DIII-D, EAST and others have indicated that ELM suppression and triggering depend on the amount of mass injected. Cryogenic deuterium pellets and impurity pellets of lithium have been used experimentally. Only a sufficiently large size of lithium pellet is able to trigger ELMs in EAST with 100% certainty. Additional experiments will be needed to fully characterize the mass injection with ELM signatures. Meanwhile, it is unclear whether the existing mass injection techniques are suffice to map out the all of mass-injection effects on ELM control. For example, a factor of 2 or less in experimental mass delivery uncertainty may be needed. However, once the pellet entered the plasma, the exact mass deposition is pellet-trajectory dependent. We therefore supplement experiment studies with empirical models for pellet ablation and BOUT++ nonlinear multi-field MHD simulations of ELM triggering. The existing technique for disruption mitigation in DIII-D is included as a possible candidate for hollow pellet injection.

2. ELM TRIGGERING & ABLATION MODELS

The ELM triggering involves multiple physical processes. We may separate the triggering process into pellet delivery, pellet ablation, and pellet-induced plasma propagation, taking advantage of the separations in temporal scales involved in ELM triggering.

2.1. Ablation models

Plasma ablation of a pellet leads to the formation of a neutral cloud, which is subsequently ionized. The ionized atoms from a pellet propagate along the local magnetic flux tubes, justifying the assumption that mass deposition is local to a flux tube in a magnetized plasma. The amount of mass deposited onto the flux tube is given by

$$N_{ab}(r) = \int \frac{dN}{dt} dt \sim < \frac{dN}{dt} > \frac{\Delta}{v_p}, \tag{1}$$

where <dN/dt> is the average ablation rate, Δ the width of the flux tube and v_p the pellet speed. v_p is assumed to be a constant determined at the injector. The average ablation rate dN/dt (we remove the averaging '< >' symbol from now on for simplicity) can be in general written in the form [6,7]

$$\frac{dN}{dt} = K n_{e0}^{k_1} T_{e0}^{k_2} r_p^{k_3}, \tag{2}$$

where the coefficient K and the exponents k_1, k_2, k_3 for electron density n_{e0} (prior to the pellet ablation), temperature T_{e0} (prior to the pellet ablation) and pellet radius r_p at the time of ablation depends on the microphysics of ablation.

2.2. ELM triggering mechanisms

In the linear ideal MHD model, an ELM is triggered when the peeling-ballooning (P-B) mode becomes unstable and leads to a growth rate $\gamma > 0$ [8]. In the nonlinear models and simulations [9, 10], the triggering threshold becomes $\gamma > \gamma c$, with $\gamma c \sim 0.1/\tau_A$ and τ_A being the Alfven time. Furthermore, JOREK simulations also showed that ELM triggering by pellet injection is correlated with the toroidally localized high edge pressure regions when the localized particle density increases due to pellet ablation. Subsequent increase in pressure is due to ionized pellet particle heating by the ambient plasma [11]. Recent simulations using BOUT++ came to similar conclusions [12]. When the pressure in this localized edge region exceeds a threshold, ballooning modes grow non-linearly leading to ELM crash. In addition, the effects of the local electric field can not be ignored. In short, the BOUT++ modeling motivates an empirical density threshold for ELM triggering N_{th} given by

$$N_{th} = \kappa_1 a_0 R_0 \Delta n_{e0}, \tag{3}$$

here $\kappa_1 > 1$ is the threshold parameter for ELM triggering. a_0 is the minor radius, R_0 is the major radius, Δ the radial width of the ablation cloud, as given in Eq. (1), and n_{e0} the local electron density before the pellet ablation. For $R_0 = 1.67$ m and $a_0 = 0.67$ m, $n_{e0} = 5\times10^{18}$ m^{-3}, κ_1 is found to be about 60 times the local plasma density. Correspondingly, $N_{th} = 1.7\times10^{18}$ or the same number of atoms in a lithium solid sphere with a radius around 200 μm.

3. MASS DELIVERY & CORE IMPURITIES

In an ITER type-I ELMy H-mode plasma, electron density and temperature are 4×10^{19} m^{-3} and 500 eV at the separatrix, and 8.7×10^{19} m^{-3} and 4 keV at the top of the transport barrier. The pedestal width is assumed to be 6 cm. Below, we pick a plasma condition similar to some of the parameters and use it to examine ELM pacing using hollow pellets. Two types of non-fueling pellets are compared, lithium and boron.

It's been experimentally observed that, in addition to pellet size, ELM triggering also depends on pedestal parameters. To reliably trigger an ELM, the pellet needs to be sufficiently large (and fast) to penetrate close to the pedestal top [13]. The pedestal dependence of ELM triggering potentially poses an issue in potential core contamination when using a normal solid-core pellet as illustrated in Fig.1.

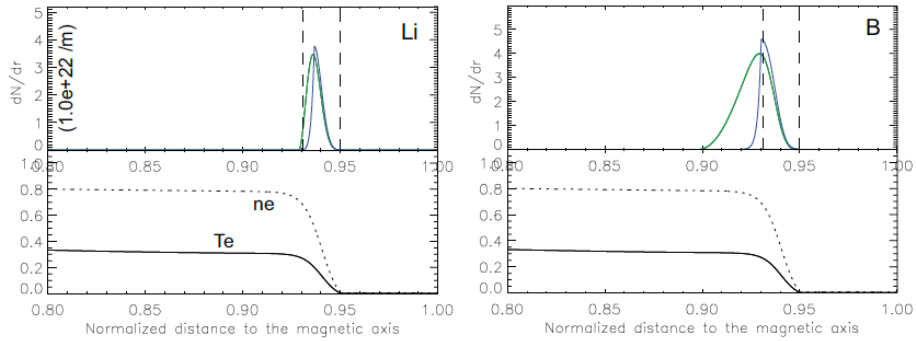

Figure 1. Comparison of mass deposition of a normal solid-core pellet and a hollow pellet. Hollow pellet can achieve similar mass deposition while minimizing core plasma contamination. Pellet initial radius is 1 mm, initial velocity 500 m/s. The core plasma temperature 4 keV, core density 8×10^{19} m^{-3}. The separatrix density is 10^{18} m^{-3} and temperature of 30 eV. The pedestal width is 2% of the minor radius.

3.1. Core impurities

One benefit of inducing ELMs at frequencies higher than the natural ELM frequency is to prevent the buildup of plasma core impurities. On the other hand, there are concerns for ELM pacing using pellets from impurities control perspectives [14]. The mass limit has been estimated as function of the atomic number Z, as shown in Fig. 2.

3.2. Pellet penetration

We shall consider pellet penetration at the constant initial injection velocity and ignore acceleration due to ablation and other plasma-pellet interactions. For the fixed pellet radius of 1 mm, the mass deposition as a function of pellet injection velocity is shown in Fig.3. For the fixed pellet injection velocity of 1 mm, the mass deposition as a function of pellet radius is shown in Fig.4.

3.3. Optimal hollow pellet dimensions

Based on the above, the dimensions of an optimal spherical hollow pellet at a fixed injection velocity v_p, {\it i.e.}, its initial radius and thick, are determined by the following factors: the pedestal plasma condition, the amount of mass required to trigger an ELM, the tolerable impurity levels, and the atomic number. The total hollow pellet mass is therefore given by

$$M_h = M_1 + M_2 + M_3, \tag{4}$$

where M_1 = N_{th} m_0 is determined by the ELM triggering threshold, with N_{th} given by Eq. (3) and m_0 the atomic mass of the pellet. M_2 is determined by the pedestal plasma condition and M_3 by the impurity tolerance level. In the case studies as in Fig.1, the hollow pellet shell thicknesses (T_h) are found to be 325 μm (B) and 2112 μm (Li) respectively for v_p = 200 m/s. At v_p = 400 m/s, one finds that a boron hollow spherical shell thickness to be 163 μm and lithium hollow shell thickness to be 1056 μm. For a fixed N_{th} = 10^{19}, 10^{20} and 10^{21}, The optimized pellet radius is summarized for Li and boron in Fig. 5.

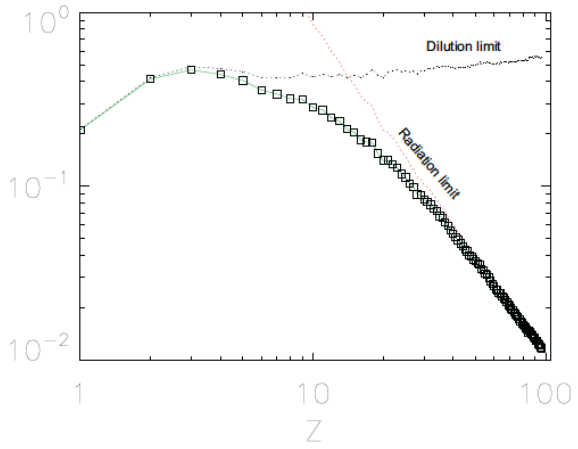

Figure 2. The mass limits for different elements using an ITER-like impurity fraction scaling in '□' symbol. The two dashed lines (color coded) correspond to the dilution and radiation limit. respectively. The mass limit for lithium is 0.49 mg, for boron is 0.46 mg.

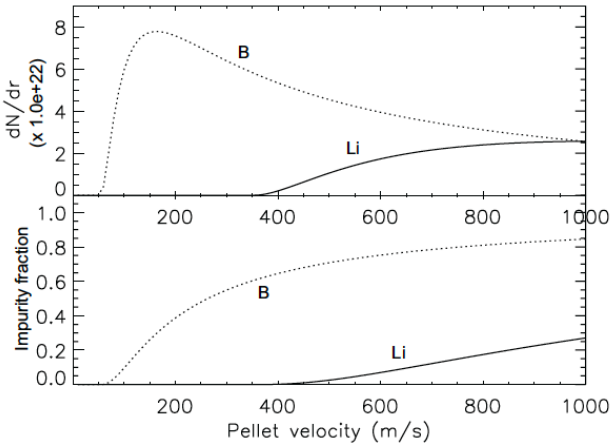

Figure 3. For fixed pellet radius r_p = 1 mm and fixed pedestal conditions, (Top) the mass deposition (dN/dr) as a function of Li or B solid sphere injection velocity. (Bottom) The fraction of the solid spheres that reach beyond the optimal ELM triggering location as a function of injection velocity.

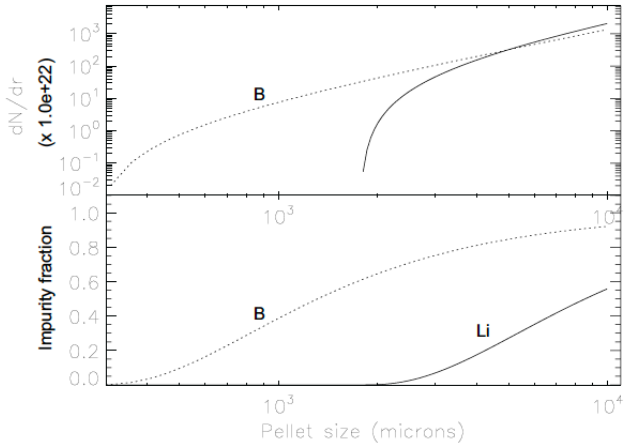

Figure 4. For fixed pellet velocity $V_p = 200$ m/s and fixed pedestal conditions, (Top) the mass deposition (dN/dr) as a function of Li or B solid sphere size (radius). (Bottom) The fraction of the solid spheres that reach beyond the optimal ELM triggering location as a function of solid sphere size.

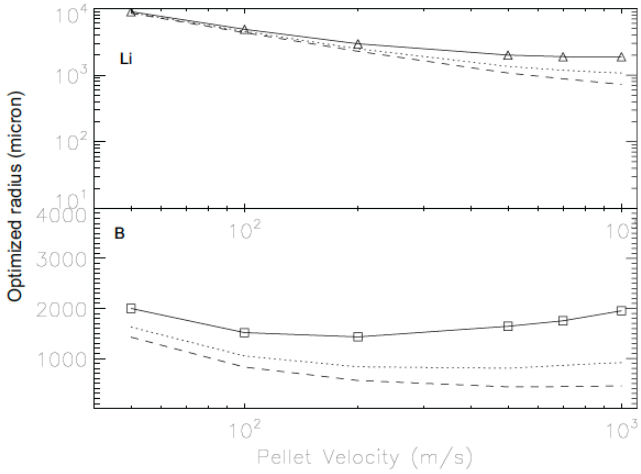

Figure 5. Optimal hollow pellet initial radius depends on the atomic number, injection velocity, pedestal condition. The calculated Li and B radius as a function of injection velocity for fixed pedestal conditions are shown here for different amount of material needed at the pedestal shoulder. The results also indicate that the injection can be further optimized by tuning the injection velocity.

4. HOLLOW PELLET FABRICATION

We briefly go through some existing options before summarizing the progress in developing boron hollow spheres.

4.1. Some existing options

Various hollow spherical targets have been developed for inertial confinement fusion (ICF) experiments [15-17]. Examples include hollow glass spheres, hollow polymer spheres (an example is shown in Fig. 6), hollow boron carbide spheres. While some of these targets may be directly used to magnetic fusion applications, broadening the material and structure choices are of interest for a number of reasons. The ICF targets are

designed for DT fusion under extremely high pressure for a brief time window, which is estimated to be around 10^{-11} s.

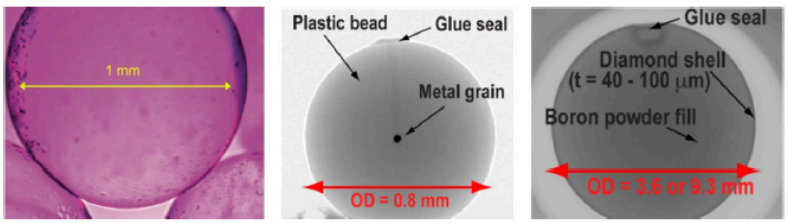

Figure 6. Examples of various core-shell pellets. (a.) Hollow polymer pellet; the shell thickness is about 20 μm. (b.) A plastic bead impregnated with a small tungsten grain; (c.) A diamond shell filled with boron powder. The diamond shell thickness is 40 μm.

Core-shell spheres have also been developed and adopted in magnetic fusion applications, see two examples shown in Fig. 6. Small hollow pellets are excellent tools for calibration of spectroscopic diagnostics in tokamaks, as a well-known quantity of the desired material can be delivered to the plasma core [18]. The shell protects the core material from ablation and loss in the launch tube and plasma edge region and ensures that the desired quantity of material to be studied reaches the core. In the DIII-D experiments [19], small (OD = 0.8 mm) plastic (poly-alpha methylstyrene, PAMS, C_9H_{10}) plastic bead pellets carrying much smaller (10 μg) tungsten grains were used to calibrate spectroscopic core tungsten measurements in support of the DIII-D tungsten divertor rings experiments. Another type of core-shell also been pursued on the DIII-D tokamak for disruption mitigation studies.

4.2. Boron spheres

A growing number of methods are being developed to make spheres and hollow spheres, for example, the microfluidic techniques [20]. We report progress with boron hollow shell development, using an approach similar to a gel-casting method described recently to make boron carbide (B_4C) hollow spheres [21]. The fabrication took two main steps. In the first step, core-shell structured B_4C was fabricated by coating molybdenum (Mo) balls with B_4C slurry. The fabricated core-shell structured B_4C microspheres exhibit a large size (2200 - 2300 μm) and a wall thickness of 100 - 180 μm. In the second step, the core-shell structured B_4C microspheres were laser drilled and the metal cores subsequent corrosion to obtain the B_4C hollow microspheres. It should be mentioned that the gel-casting technique is also suitable for the preparation of other ceramic hollow microsphere that may be of interest to magnetic fusion, including assessment of material and first wall options. We have made the first samples of boron shell with a PMMA core, as shown in Fig.7.

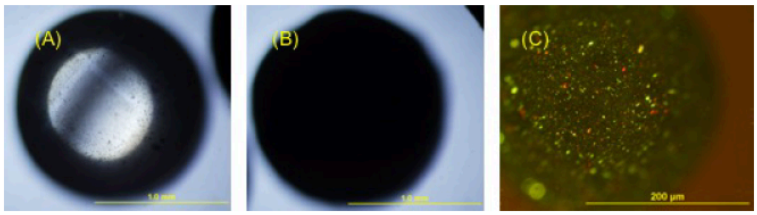

Figure 7. Images of boron-shell enclosed PMMA spheres. (a.) A PMMA sphere that is used as a template for boron coating; the sphere is 1.5 ± 0.05 mm in diameter and a sphericity of 50 μm. (b.) A boron coated PMMA sphere; (c.) The same sphere as in (b) with a higher microscope magnification.

5. EXPERIMENTAL PROGRESS

Several existing techniques can be leveraged upon towards demonstration of the new hollow pellets in magnetic fusion. One is a pellet launching system. Another is a diagnostic system that can monitor the pellet-plasma interactions in real-time with good spatial and temporal resolutions. As the first example, a pneumatic (helium pulse) launcher in DIII-D can inject pellets radially inward at velocities of 100 - 300 m/s from the outer midplane. A schematic of the experimental setup is shown in Fig.8. The pellet launcher breech is flexibly configurable to allow holding and firing of different sized pellets.

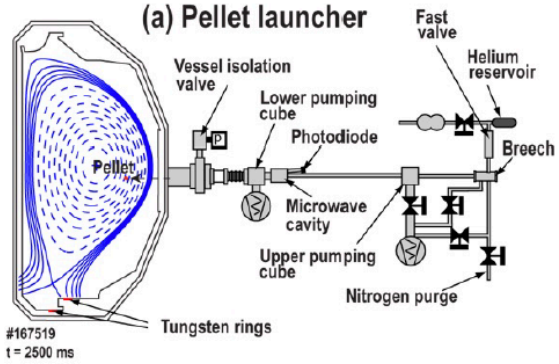

Figure 8. Schematic of a pellet launcher used for various pellet injection in DIII-D.

Recently, the launcher system was first successfully used to demonstrate the shell pellet concept for disruption mitigation in DIII-D. A picture of the pellet was shown in Fig.6, which has an OD of 3.6 mm made of diamond with a shell thickness of 40 μm. The shell is filled with boron powder. The pellet shells burnt through close to the plasma magnetic axis, releasing boron powder and causing a very rapid radiative shutdown of the plasma, as shown in Fig.9. Large hollow pellets (`shell pellets') filled with different payloads are of interest for tokamak disruption mitigation, since a precisely designed payload can be delivered to the plasma core and, ideally, satisfy the different shutdown requirements to minimize different times of wall damage that can result from disruptions, such as localized heat loads and vessel forces. Previous shell pellet disruption mitigation experiments have had challenges getting payload deposition into the core during the disruption, as the pellets have either passed completely through the plasma without breaking open or have broken in the plasma edge or have not caused a rapid shutdown [22]. Future work will continue to study the use of shell pellets for disruption mitigation in DIII-D for application in future large tokamaks like ITER and DEMO.

For the in-situ diagnostic of a hollow-pellet-plasma interaction, we may use a recently demonstrated dual-filter imaging technique [23], the structures of pellet ablation is resolved using the new technique. The imaging technique can be used in conjunction with a hollow-pellet injection experiment.

6. SUMMARY & CONCLUSIONS

Precise delivery of mass to magnetic fusion plasmas is a problem of growing interest. We used various empirical models for ablation, augmented by BOUT++ simulations, to assess the concept of hollow pellets for ELM applications in magnetic fusion. Hollow sphere for precise ELM control is possible with significant reduction of impurity contamination in the core. Prototype core-shell boron spheres have been fabricated. Additional applications of hollow spheres in diagnostics and fueling are also possible.

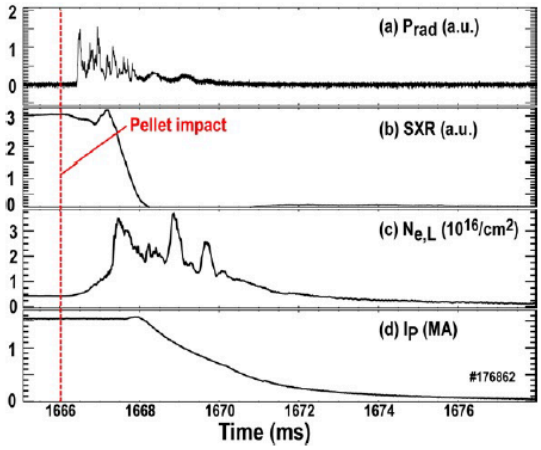

Figure 9. Example of rapid shutdown with large (OD = 3.6 mm) shell pellet showing rapid radiative shutdown. Time traces are shown of (a) radiated power, (b) SXR brightness (showing collapse of thermal energy), (c) electron line density (showing deposited impurities) and (d) plasma current (showing decay of magnetic energy).

ACKNOWLEDGEMENTS

We thank Peter Goodwin (Los Alamos National Laboratory) in helping with imaging of the boron spheres. This is work is supported in part by US DoE/Fusion Energy Sciences for US/China Long Pulse Tokamak collaboration.

REFERENCES

[1] Zinkle S. J. et al, Fusion. Eng. Des. 89 (2014) 1579-1585.
[2] Federici G. et al, Nucl. Fusion 41 (2001) 1967-2137.
[3] Naujoks D. Plasma-Material Interaction in Controlled Fusion (Springer, 2006).
[4] Wang Z. et al, Physics of dust in magnetic fusion devices , in New Aspects of Plasma Physics (2007) 394-475.
[5] Wang Z. et al, J. Plasma Phys. 82 (2016) 615820202.
[6] Parks P. B. et al, Nucl. Fusion 28 (1988) 477.
[7] Sergeev V. Yu et al, Plasma Phys. Rep. 32 (5) (2006) 398-412.
[8] Snyder P. B. et al, Phys. Plasma. 9 (2002) 2037.
[9] Xu X. Q. et al, Phys. Rev. Lett. 105 (2010) 175005.
[10] Xi P. W. et al, Phys. Rev. Lett. 112 (2014) 085001.
[11] Huysmans G. T. A. et al 2009 Plasma Phys. Control. Fusion 51 124012
[12] Wang Y. M. et al 2018 Nucl. Fusion (*submitted*).
[13] Lang P. T. et al , Nucl. Fusion 51 (2011) 033010.
[14] Loarte A. et al , Nucl. Fusion 54 (2014) 033007.
[15] Hoppe M. Fusion Technol. 38 (2000) 42.
[16] Nagai K. et al. J. Plasma Fusion Soc. 80 (2004) 626.
[17] Du K. et al , Matt. Rad. Extr. 3 (2018) 135.
[18] Sudo S. and Tamura N. Rev. Sci. Instrum. 83 (2012) 023503.
[19] Hollmann E. M. et al., Rev. Sci. Instrum. 88 (2017) 103501.
[20] Nisisako T. Curr. Opin. Colloid Interface Sci. 25 (2016) 1.
[21] Chen R. et al , Ceramic International 43 (2017) 571.
[22] Hollmann E. M. et al., Phys. Plasmas 17 (2010) 056117.
[23] Sun Z. et al Rev. Sci. Instrum. (accepted for publication , 2018).